# Implementation of a borescopic technique in a conical spouted bed for tracking spherical and irregular particles

Aitor Atxutegi, Mikel Tellabide, Gartzen Lopez, Roberto Aguado*, Javier Bilbao, Martin Olazar

*Dept. of Chemical Engineering, University of the Basque Country UPV/EHU, PO Box 644 – E48080 Bilbao, Spain*

## Abstract

A methodology based on the borescopic technique has been developed and validated for tracking solid movement within a conical spouted bed. The procedure developed and fine-tuned allows monitoring the descending and ascending optical flow of both spherical and irregular particles in the annulus (dense zone) and spout (dilute zone) in the bed. A high speed camera (up to 16000 fps) fitted with a fiber optic continuous light source was used for recording, and an image treatment algorithm modified and adapted to account for differences in particle shape and bed density (dilute or dense) was applied to the registered data. The procedure allows gathering information on the velocity of particles in a wide range of sizes, from a few millimeters ($\bar{d}_p = 7$ mm) to micrometers ($\bar{d}_p = 93$ µm).

*Keywords:*

Particle tracking, image treatment, borescopic high speed $PIV$, conical spouted bed

*Corresponding author

*Email address:* roberto.aguado@ehu.eus (Roberto Aguado)

## 1. Introduction

Gas-solid contact regimes play an essential role in a wide range of processes in the chemical industry due to their flexibility concerning operating conditions and their capability to achieve high heat and mass transfer rates. Unlike fixed and fluidized beds, spouted beds are specifically suitable for handling coarse and irregular particles. Moreover, some improvements have been recently proposed for handling fine materials and those with wide particle size distributions. Thus, the joint use of draft-tubes[1, 2, 3] and a new fountain confiner[4, 5] is worth mentioning. These internal devices highly improve the flexibility and potential applications of this contact technology. This way, the application of conical spouted beds and other spouted bed designs has been studied in several chemical processes, such as polymerization[6, 7], gasification[8, 9], pyrolysis[10, 11], torrefaction[12], chemical vapor deposition[13] and combustion [14]. Nevertheless, the above mentioned applications of spouted beds are mainly limited to laboratory scale units[15], which emphasizes the need to understand the internal hydrodynamic behavior of the system prior to its industrial implementation. Simulation models are a useful tool to reduce the costs involved in the design, construction and operation of pilot and commercial units. In fact, $CFD - DEM$ techniques are becoming popular[16, 17, 15, 18, 19], as they allow attaining promising results for a correct understanding and implementation of the technology. However, these types of dynamic models require very detailed experimental data involving particular setups to make accurate estimations of the properties under study.

Solid velocity along with local porosity are of uttermost significance in gas-solid contact systems, as they are key factors influencing other relevant properties in the bed, such as segregation, pressure drop, temperature, gas and solid residence times, heat and mass transfer rates and cycle times. In addition, local measurements in the bed are essential in order to compare systems from different research groups[20], given that they are usually operated under slightly different configurations and so direct comparison of hydrodynamic properties, such as pressure drop and minimum spouting velocity, can be cumbersome.

The acquisition of such data in fluidized beds is a challenge that has been approached by means of either non-invasive and invasive techniques, recently revised in detail by Hatamipour et al.[18]. Amongst the former, those based on particle optical monitoring[21], X-ray volume tomography[22], capacitive volume tomography[23], ultrafast X-ray computed tomography[24], gamma ray computed tomography[25], radioactive particle tracking[26, 27] and magnetic particle tracking[28, 29] are worth mentioning. The use of invasive techniques is suitable whenever probes are of small size and when the influence of the device on the overall hydrodynamics is insignificant, as when the reactor is of considerable volume[30]. Concerning the use of invasive techniques in the current reactor Olazar et al.[31] proposed a device based on an optical fiber probe to measure local properties but required calibration for each material type. Nowadays, one promising invasive technique is the borescopic high speed particle image velocimetry ($PIV$)[32], which is a natural evolution of the traditional pseudo $2D$ velocimetry studies[33]. This technique enables real time monitoring of the flow inside the bed[34], does

not require any modification for high volume systems and allows registering local properties with sampling frequencies well above the natural oscillation frequency of 4-8 Hz[35] encountered in spouted beds. Borescopic high speed $PIV$ has been successfully used in fluidized columns[36] and risers[37]. The image treatment in these studies ranges from gray scale thresholding for bubble identification[38] to the more complex edge detection labeling and Gaussian cross correlation[37] for individual particle identification.

The aim of this study is to demonstrate the capability of the borescopic technique for the monitoring of solid flow in the different regions of spouted beds (annulus and spout) operating under a wide range of conditions and solid flow patterns, i.e., fine and coarse particles under low and high spouting velocities. Nevertheless, image recording and processing in these beds involves difficulties due to the highly heterogeneous porosity profiles depending on the bed zone and spouting regime. A robust enough algorithm is therefore required to switch from one option to the other depending on the local porosity and, furthermore, it should be valid for any type of material under study in the conical spouted bed, without having to rely on specific bed porosity ranges for the gray scale thresholding.

## 2. Experimental setting and methods

### *2.1. Experimental equipment*

The pilot plant is composed of a blower, flow meter, pressure drop gauge, contactor, filter and cyclone. The blower has a power of 5.5 kW and supplies the air required for bed spouting. Gas flow rate is measured by means of a thermal mass flow meter, which is used in the 0-600 $\mathrm{Nm^3\,h^{-1}}$ range.

The blower supplies a constant flow rate, so the gas fed into the contactor is controlled by either acting on a motor valve that reroutes the remaining air to the outside or changing the frequency of the blower motor. The pressure measurements are carried out by means of two pressure taps, which are inserted at the inlet and output pipes of the contactor. Moreover, an air filtering system is located downstream the contactor in order to retain fine particles before the outlet air stream is released to the environment.

The main component of the experimental unit is the contactor, Figure 1, which has a conical geometry. The unit allows operating with contactors of different geometries, but in this work only one contactor made of $PET$ has been used. Figure 1 shows the geometric factors of this contactor, which are as follows: column diameter, $D_c$, 0.36 m, contactor angle, $\gamma$, 36°, height of the conical section, $H_c$, 0.45 m, base diameter, $D_i$, 0.068 m, and gas inlet diameter, $D_o$, 0.04 m.

This contactor allows fitting internal devices in order to improve the hydrodynamic stability of the bed. In this study, an open-sided draft-tube has been located along the axial position of the contactor. Its performance has already been studied for sand and glass beds in previous studies and the results are reported elsewhere[1, 39, 40, 4, 2]. One of such devices is the open-sided draft tube, with its characteristic aperture ratio, $\omega_T$, which greatly influences the hydrodynamic performance of the bed. Thus, an increase in the aperture ratio favors the incorporation of solid into the spout, promoting its circulation[39]. The main dimensions of the draft-tube are as follows: aperture ratio, $\omega_T$, 57%, tube diameter, $D_T$, 0.04 m, and tube length, $L_T$, 0.20 m.

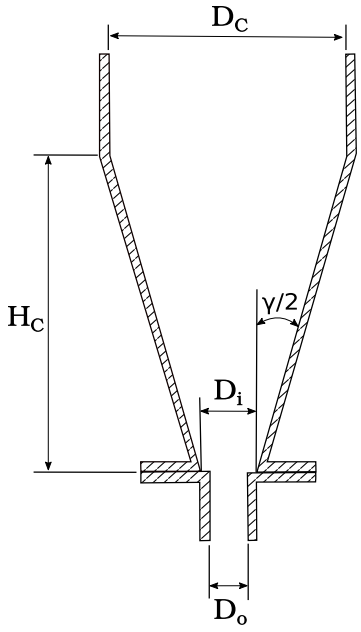


Figure 1: Scheme of the conical spouted bed contactor.

Another internal device of uttermost significance is the fountain confiner, specially when a stable spouting regime is required with fine and ultra-fine solids[4]. This device is a cylindrical $PET$ tube with the upper outlet closed and is located along the axis above the bed surface. Accordingly, the elutriation of solids is avoided or greatly reduced and the range of flow rates for stable spouting widens[5]. The diameter of the device is 0.2 m, the length of the tube is 0.5 m and the distance between the lower end of the device and the bed surface is 0.06 m.

*2.2. Experimental conditions*

Experiments with fine and coarse particles have been performed in order to cover a wide range of solid flow patterns and porosities. It should be noted that the spouting behavior of fine and coarse materials is significantly

different. Thus, coarse materials are characterized by stable spouting regimes with low and dense fountains (Figure 2(a)). Stability problems commonly arise operating with fine materials and, as stated above, the incorporation of draft-tubes has been regarded as a suitable solution for the stabilization of these beds [1, 39, 41]. Nevertheless, the spouting of fine particles with draft-tubes is characterized by high fountains, which usually lead to elutriation. The use of a fountain confiner, Figure 2(b), has proven to be efficient to avoid this problem, which in turn also improves bed stability[4]. Furthermore, it allows for operating under vigorous regimes with gas velocities well above the minimum spouting velocity, which are required in certain applications, such as drying[5] and biomass gasification[42]. Draft-tube and fountain confiner were used for the spouting of fine solids, whereas none of these devices was required for a suitable spouting of coarse materials. As shown in Table 1, two materials have been used in this study, sand as a reference for irregular fine particles and glass beads as a reference for sphere like coarse particles. The latter ($\bar{d_p} > 1$ mm) correspond to group $D$ of Geldart classification, whereas the sand is classified as Geldart $B$ type.

Table 1: Properties of the materials used.

| Material | $\rho_b$ (kg m$^{-3}$) | $\bar{d_p}$ (mm) | Shape | Geldart classification |
|---|---|---|---|---|
| Glass beads | 2500 | 2 | Regular | $D$ |
| Sand | 2420 | $93 \cdot 10^{-3}$ | Irregular | $B$ |

The initial bed height, $H_o$, in both experiments has been kept at 20 cm in order to line up with the draft-tube required for stable spouting with sand particles. These beds account for masses of 4.6 and 5.2 kg of glass beads

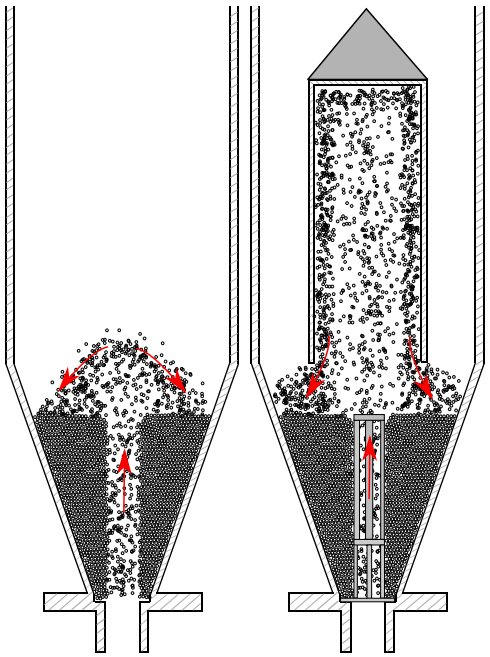

(a) (b)

Figure 2: Fountain shape for (a) glass beads, and (b) fine sand with draft-tube and fountain confiner.

and sand, respectively. In the experiments performed with glass beads, a gas flow rate of 143 $m^3\,h^{-1}$ was used, corresponding to a gas velocity/minimum spouting velocity ratio, $u/u_{ms}$, of 1.1. The gas flow rate operating with fine sand was of 80 $m^3\,h^{-1}$, $u/u_{ms} = 4.0$, which promotes the development of a vigorous spouting regime with a high fountain.

*2.3. Borescopic technique*

As shown in Figure 3, the experimental setup is composed of a camera, a borescope, a camera displacement system and a light source. The camera is a *AOS S-PRI* (AOS Technologies AG) with a maximum recording resolution of 900 x 700 and a maximum frame rate of up to 16500 fps with reduced

resolution. The depth of field is 0.8 cm and starts at 5 mm from the tip of the device.

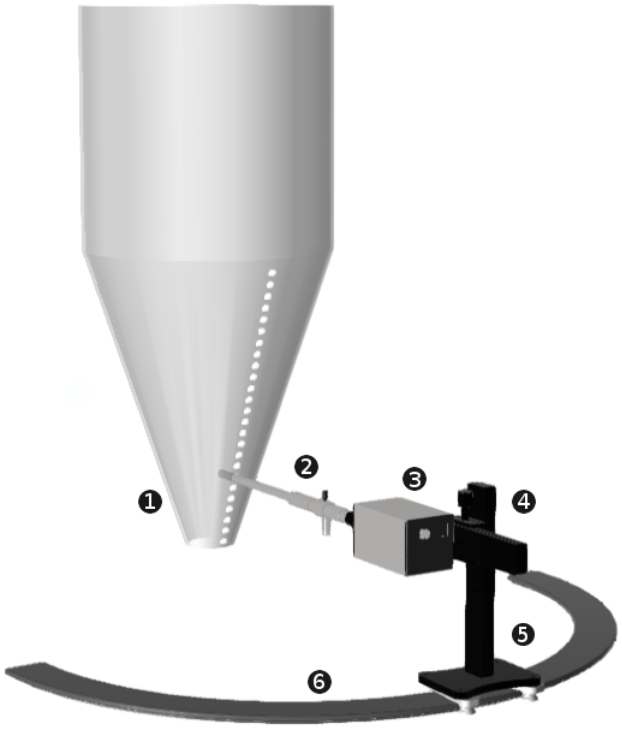


Figure 3: Image recording system: (1) Contactor, (2) borescope, (3) camera, (4) straight sliders, (5) sliding platform, and (6) perimeter slider.

The borescopic system is shown in Figure 4. It is composed of a C fitting optical adapter with an iris regulator, a borescope and a protecting cartridge. The optical adapter has a lens with an opening angle of 50°. The borescope has a length of 0.25 m and an external diameter of 0.01 m. The borescope optical fiber is connected to a continuous light source with a minimum brightens of 700 lm ($IntraLED5$). The cartridge in which the borescope is inserted is a stainless steel tube, whose tip is protected by a sapphire glass in order to

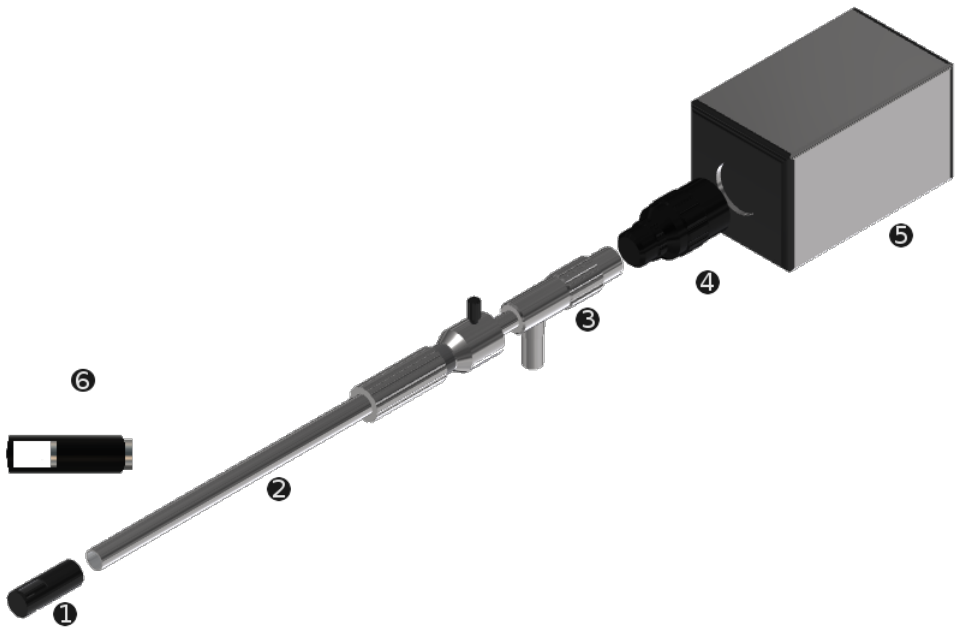


Figure 4: Borescopic system: (1) Spacer, (2) cartridge protector, (3) borescope, (4) optical adapter, (5) camera and (6) enlarged image of the spacer.

avoid its attrition by high velocity sand particles. The cartridge protrudes slightly from the borescope, which in addition to protecting the optical system also keeps the measuring point at the minimum distance to properly focus the image on the sensor. However, this distance creates a reflection on the sapphire that slightly reduces the measuring window size. Accordingly, the borescope protector is provided with a screw that allows moving the cartridge independently of the optical system, regulating this way the reflection. Finally, both the optical adapter and the borescope are provided with a lens that enables changing the focal point of the optical device to obtain a sharp image of the objects.

The camera displacement system is made up of a set of straight sliders

mounted on a rail around half the contactor perimeter with an arc diameter of 0.85 m, Figure 3. A platform fitted with two straight sliders (horizontal and vertical) runs along the rail. The camera is mounted onto the horizontal straight slider, which in turn is mounted on the vertical slider, enabling two-axial movement and measurements at any point in the contactor.

Finally, a $3D$ printed spacer is placed on the tip of the protecting cartridge, Figure 4. This spacer has been printed using black thermoplastic polyurethane ($TPU$) and configured in a way that the background gives the required contrast and its sufficiently wide openings allow solids to flow through the spaces with minimum disturbance. In order to asses the minimum distance between the borescope tip and the spacer to avoid disturbances, runs have been carried out with and without the spacer. The runs in which the solid is descending allow measuring velocity without the need for any spacer, as there are no gaps in the solid flow. The distance for which disturbances are negligible is $\sim 10\, d_p$, and therefore the spacer has been placed at this distance in all the measurements in which solid velocity was measured inside the contactor. It should be emphasized that the use of this element is crucial for measuring particle velocity in the spout region, in which many solids are recorded away from the desired field depth, which causes noise and spurious detections.

Recordings have been conducted at different points located at varying levels in the annular and spout zones. The fountain has only been recorded at one level because the current setup with a single camera cannot detect displacements normal to the measuring plane, which are especially pronounced in this zone. In fact, velocity can be slightly corrected only in the case of

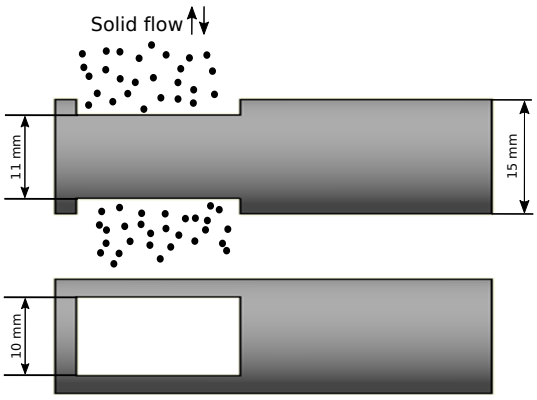


Figure 5: Diagram of the spacer with main dimensions and solid flow description.

spherical particles, for which the particle size is known. Therefore, the current setup and analysis is only valid for the spout and annular zones. Solid flow pattern in these zones differs greatly, i.e., particle velocity (magnitude and direction) and bed porosity are very different. The latter depends on the shape of the material, and especially on particle size. Thus, sand (much finer than the glass used) tends to move in clusters instead of individual solid bodies. In each bed level, particle movement has been recorded at the points of maximum and minimum particle circulation, i.e., at the axis of the contactor (located in the spout) and on the wall of the contactor located in the annulus zone.

### *2.4. Image processing*

The image treatment algorithm is written in *Matlab* 2017*b* and described in Figure 6. It is designed to detect particle velocities for most materials commonly used in hydrodynamic studies, with a detection range that covers both spherical and irregular particles, as well as a wide range of particle sizes; i.e., $\bar{d_p}$ of 4 mm for glass beads, 70 µm for *FCC* catalysts or fine sand.

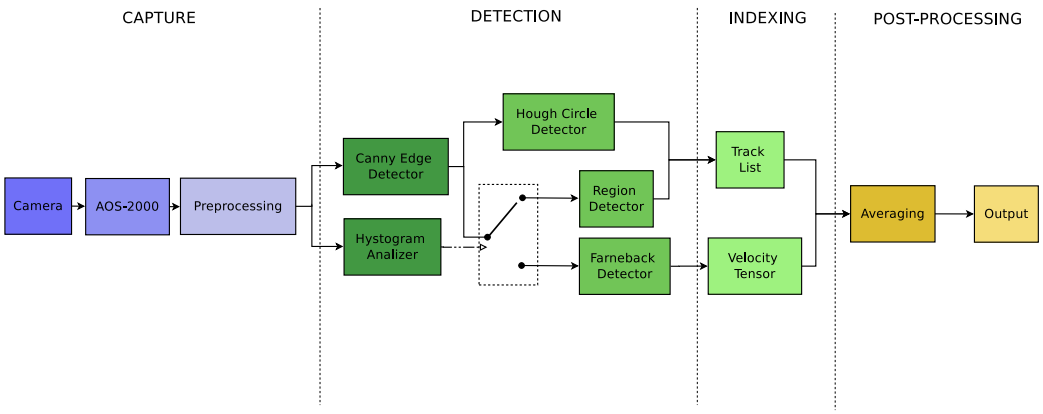


Figure 6: Flowchart for particle detection and image treatment algorithm.

In order to ensure a correct image capture and velocity measurement, the image treatment procedure has been split into the four steps shown in Figure 6. The first step is image capture, in which the correct light brightness in the borescope, as well as the capture speed and the sensible shutter speed, are set. Once the camera has taken about $2.5\,s$ footage, the videos are preprocessed by cropping each image to remove the reflective ring and correct the lens distortion. Dynamic histogram equalization is then conducted to increase the contrast between the solids and the background. Once the preprocessing has been completed, the routine has two options depending on whether solids are spherical or irregular in shape.

In case the solids are close to spherical-shaped materials, the procedure to detect their velocity is based on a canny edge detector fed into an Hough circle detection algorithm, which searches for spheres of radii within a preset pixel range and, subsequently, gives the location of the centroid of the projected circles along with the radius of each detection. The centroid location is sent to the indexing process whilst the radii give information on the particle

displacement in the normal direction to the sensor. This latter information is important to reduce the detection error by correcting the velocities for normal displacements relative to the camera. Such correction can only be applied to spherical particles, as the shape to be projected on the sensor is foreknown.

The procedure for measuring irregular particle velocities differs considerably from the spherical one. In the spout zone, solids are in a dilute phase and the edges of individual particles may be easily defined, whereas in the annular zone particle edges are hardly distinguishable from one another. In the dilute regime, the algorithm implements a canny edge detection followed by an erode-dilate routine, which identifies closed regions as individual particles, and then locates and stores the centroids and surface projections of the regions. These detections are fed into a list of tracks, similar to those used for spherical particle detections, in which particles are stored and their velocities calculated based on subsequent detections. When particles ascend through the spout in a cluster, or descend along the annulus, the algorithm fails because no single regions can be closed through the dilate-erode routine, and so there is hardly any individual detection. In this specific case the Farneback pyramidal algorithm[43] from *OpenCV* has been found to be especially suitable to average edge movements, assuming the lightning conditions are kept steady enough and that particle rotations are kept to a bare minimum. In the annular zone, particles tend to move in packs, rotations are greatly reduced and the relative displacement of one particle from the other is almost negligible, and in the spout region light is scattered in a way that the particle reflections do not affect the measurements allowing the Farneback

algorithm to make reasonable velocity measurements. The default Farneback parameters from *OpenCV* are 5 pyramid levels and scaling factors of 0.5 between levels. Nevertheless we have proven that 2 levels with the same scaling factor are enough.

Apart from spout and annulus, spouted beds contain a transition zone between these two regions, in which there is a mixture between particle clusters and fluid bubbles. Given that this zone changes from one phase to the other throughout time, a suitable switch detection procedure must be implemented. In order for the algorithm to be invariant to the average lightning level, the shape of the grayscale image histogram has been used as the main switching criterion.

The reason to choose this particular distribution is that the histogram might be either right or left tailed depending whether the brightness is increasing or decreasing between frames. The evolution of the histogram according to the different regimes is shown in Figure 7. As frames go from a densely packed region to a dilute one, the tail of the histogram is more pronounced until an almost flat distribution is attained. In this evolution, the $\alpha$ and $\beta$ shape parameters evolve from relatively high and similar values to lower ones differing greatly (the switch is activated), and finally to low and similar values, Figure 7. As observed in Figure 7, when a unimodal normal distribution is obtained, this means the packing is dense and the beta distribution parameters of best fit take high values (8.35 and 9.72). As the bed loosens and voidage increases, a left tail appears and $\alpha$ and $\beta$ decrease at different rates (the gap between them increases) (5.28 and 3.91). When a dilute regime is achieved, a flat distribution as that in Figure 7 is obtained,

with shape parameters being close to 2. Based on this switching technique, the Farnerback algorithm is used when the distribution is normal and the region detection algorithm when the distributions is flat or tailed.

$$f_X(x) = \frac{1}{B_{\alpha,\beta}} x^{\alpha-1}(1-x)^{\beta-1} \tag{1}$$

$$B_{\alpha,\beta} = \int_0^1 t^{\alpha-1}(1-t)^{\beta-1} dt \tag{2}$$

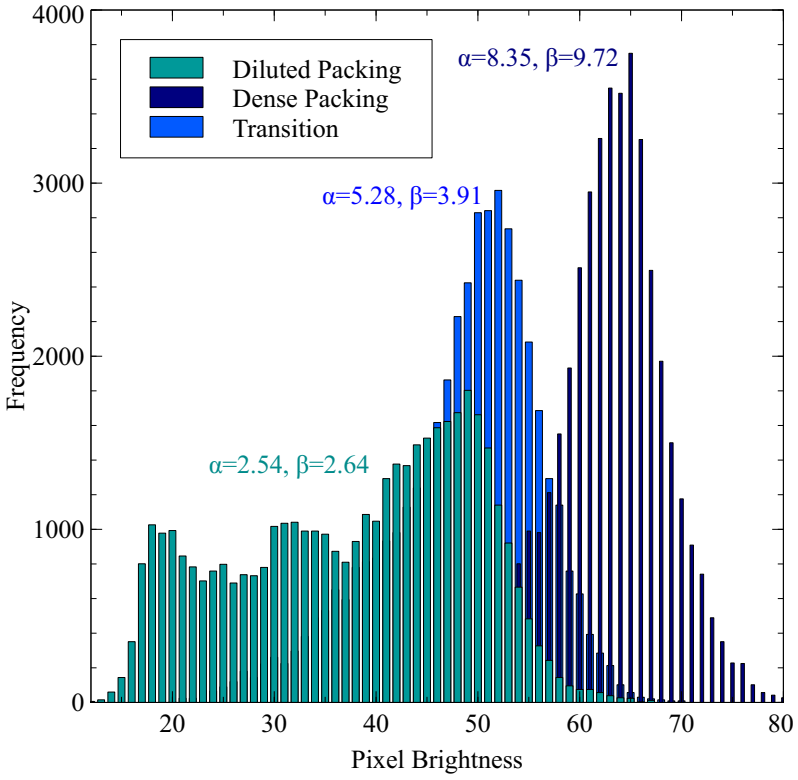


Figure 7: Evolution of frame histograms according to solid packing.

Once the detection step has been completed, the indexing step assigns individual detections in consecutive frames through the minimum cost Hun-

garian assignment algorithm, using the Cartesian distance as the cost function. These distances are only considered if they fall below a maximum displacement value that is feasible at this sampling point. In this work, the assignment of the maximum distance is corrected (specially in the spout region) based on the acceleration monitored at the sampling point. Once the position of the same particle in two consecutive frames has been assigned, the optical flow velocity calculation is straightforward.

When closely packed irregular materials are being monitored and Farnerback algorithm is used, there is no need for the mentioned assignation procedure and the velocity tensor is directly determined from the *OpenCV* software. Given that the error in determining velocities following Farnerback algorithm is higher in the frame edges, Gaussian ponderation is used to determine the average frame value.

The average particle velocity is obtained as the mean value of all the frame velocities in the recording. Frame velocity is the average of the detections (particle velocities) in a given frame. Instant particle velocities are determined based on a given frame and the previous one.

## 3. Results

### *3.1. Validation of borescopic technique*

In order to validate the results obtained with the borescopic technique and image treatment algorithms, two different strategies have been followed for dense (annulus) and dilute (spout) regions. A vertical pipe was used for the low velocities corresponding to the dense zone. Particles were fed into the pipe through an inlet located at its top and withdrawn through a hole at the

bottom. Accordingly, after a couple of seconds the solid descending velocity remains almost constant, and therefore the solid reference velocities (experimental values in Figure 8) can be calculated. These values are obtained by manually labeling the centroids and identifying particles in consecutive frames. These velocities are also compared with those obtained based on the time the solids require to travel the diameter of the borescope, which is a known value. The same procedure was followed for different solid descending velocities, which are obtained by changing the size of the whole at the bottom.

The calibration for velocities higher than those that may be attained with the aforementioned device has been conducted at the spout region itself. The experimental values in this region have been calculated from the distance traveled by the particles between two consecutive frames. The reference experimental values are those calculated by manually detecting and assigning solids in consecutive frames and have been compared with the values given by the algorithm. The reference velocity values have also been checked by comparing with the velocities obtained based on the time particles take to travel the distance of the borescope diameter, and no significant differences have been measured.

Use of these two procedures allows covering the whole range of velocities expected in the conical spouted bed. Therefore, the degree of uncertainty of the measuring technique was ascertained by comparing the experimental values with those obtained using the algorithm for the three situations (detection modes) analyzed, i.e., irregular particle (fine) dense phase, irregular particle (fine) dilute phase and coarse particle (spherical) beds, Figure 8. The

measurement of fine irregular particle velocities in the dense phase, based on the Farneback algorithm, is shown in green dots in the lower range of velocities, and they correspond to the annular region of fine sand beds. This algorithm is also preferred for clusters of fine particles ascending through the spout, due to corresponding low porosities. For velocities of up to 6.5 $\mathrm{m\,s^{-1}}$, bubbles and instabilities are more common, and therefore the algorithm for the dilute phase is used.

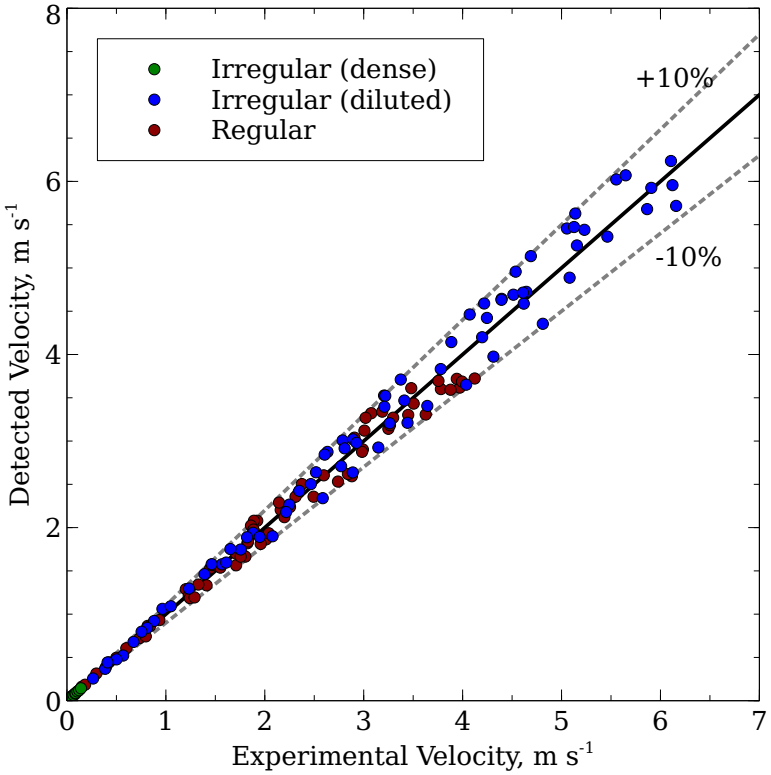


Figure 8: Parity chart of velocity detections.

The detection of spherical particles does not depend on porosity and is only influenced by the light shine upon the particles, which is optimized

based on the camera shutter speed. Accordingly, their detection covers most of the velocity range in Figure 8, with a maximum velocity detection of 4.5 $\mathrm{m\,s^{-1}}$. The maximum velocities detected for the coarse particles were always lower than those in the fine particle dilute phase, which is due to the lower acceleration rate of the larger spherical particles. As observed in Figure 8, velocity measurement errors are always below 10% of the nominal value, which is evidence that the algorithm provides reliable measurements of particle optical velocities, and therefore may be used as a suitable tool to measure local velocities in the conical spouted bed operating in a wide range of solid flow conditions.

*3.2. Velocity measurements in the spouted bed*

Once the validation has been completed velocity measurements have been conducted inside the conical spouted bed through said algorithm. Figure 9 shows a set of detection examples for the three situations corresponding to the two materials in dense and dilute phases. Figure 9(a) shows a shot taken in the annular zone when coarse glass beads are used in a conical spouted bed in which 143 $\mathrm{m^3\,h^{-1}}(u/u_{ms} = 1.1)$ of air have been fed into the contactor. Given the particle size and the optics of this setting, the number of detections (particles) in each frame ranges from 2 to 5 in a packed bed. This small number of particles makes the averaging to be greatly influenced by collisions, as they lead to a decrease in the velocity of individual particles.

Figure 9(b) shows a shot of fine irregular particles in a dilute phase taken in the spout of a $\bar{d_p} = 100$ µm fine sand bed when an air flow rate of $u/u_{ms} = 4.0$ has been fed into the contactor. The detections in this situation depend on bed porosity, but the number of detections and subsequent assignments

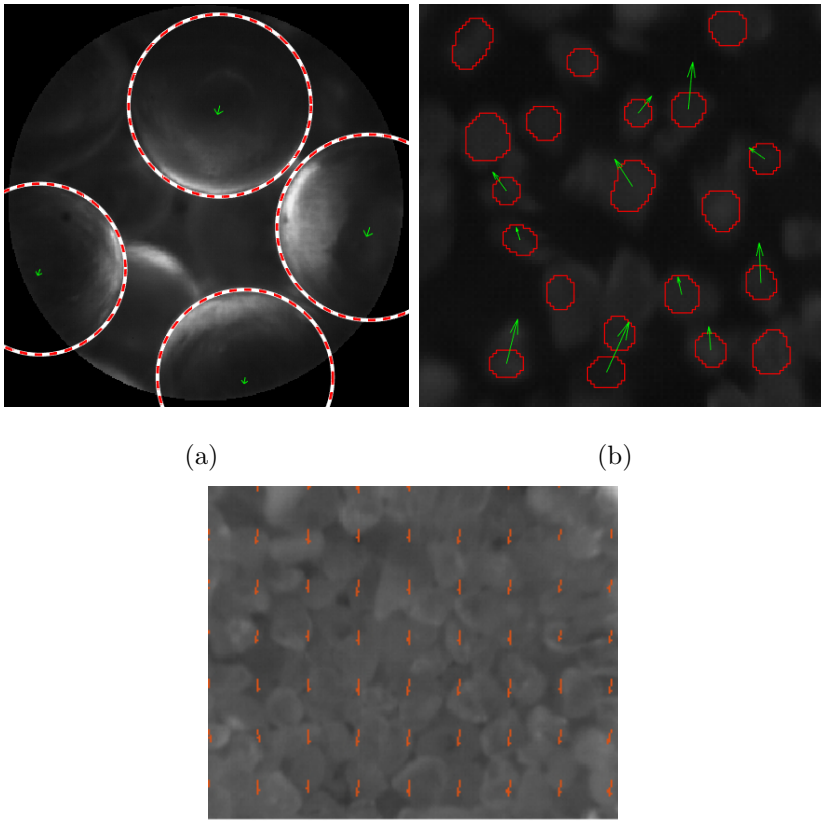


Figure 9: Detection at 20 cm from the base of the bed. (a) spherical $\bar{d_p}$ = 4 mm glass beads in the annular zone, (b) $\bar{d_p}$ = 100 µm fine sand in the spout and (c) densely packed fine sand in the annular zone.

(green arrows) are high compared to the spherical particles, Figure 9(a), which makes the velocity signal more stable.

Figure 9(c) shows a shot of the same material in the annular zone, in which a packed bed is detected and the Farneback algorithm is used. This algorithm does not depend on individual detections, making the signal stable for configurations in which this algorithm can be applied. However, care must

be taken to remove the reflection on the edge of the shot due to the sapphire, as this algorithm relies on brightness changes to calculate the velocity tensors.

Once all the detections have been indexed and properly averaged, the mean solid velocities are plotted, which are the data required for $DEM - CFD$ model validation or any other comparison. Figure 10(a) shows the detection of individual glass bead particles as they ascend through the spout to the fountain. As observed, the mean velocity in this zone is 1.25 $\mathrm{m\,s^{-1}}$. Most values in this plot show a positive velocity, which is evidence of the upwards particle movement in the spout, and those negative ones are related to transient collisions occurring when particles move close to each other due to the incorporation of a big chunk of particles from the annulus into the spout. Figure 10(b) shows the velocity signal for glass beads in the annular region of the same system. The nature of this signal is clearly oscillatory (7-8 Hz) and has a negative average value, which means the solid flux is downwards, as is the case in the annular zone. Figure 10(b) shows a lower amplitude, which is due to the lower rotational movement of the particles in the annular zone due to the viscous forces between particles while moving under frictional forces. In contrast, Figure 10(a) shows a greater amplitude of the signal because the particles in this region move in a dilute phase, and therefore rotary momentum is acquired by the solids due to the gas-solid momentum exchange and/or solid-solid tangential collisions. It should be noted that this image treatment algorithm does not consider particle rotation, but only determines the net optical flow of the solid particles.

The velocity signals for the fine irregular materials are shown in Figure 10(c) and Figure 10(d). As expected, the number of detections is much higher

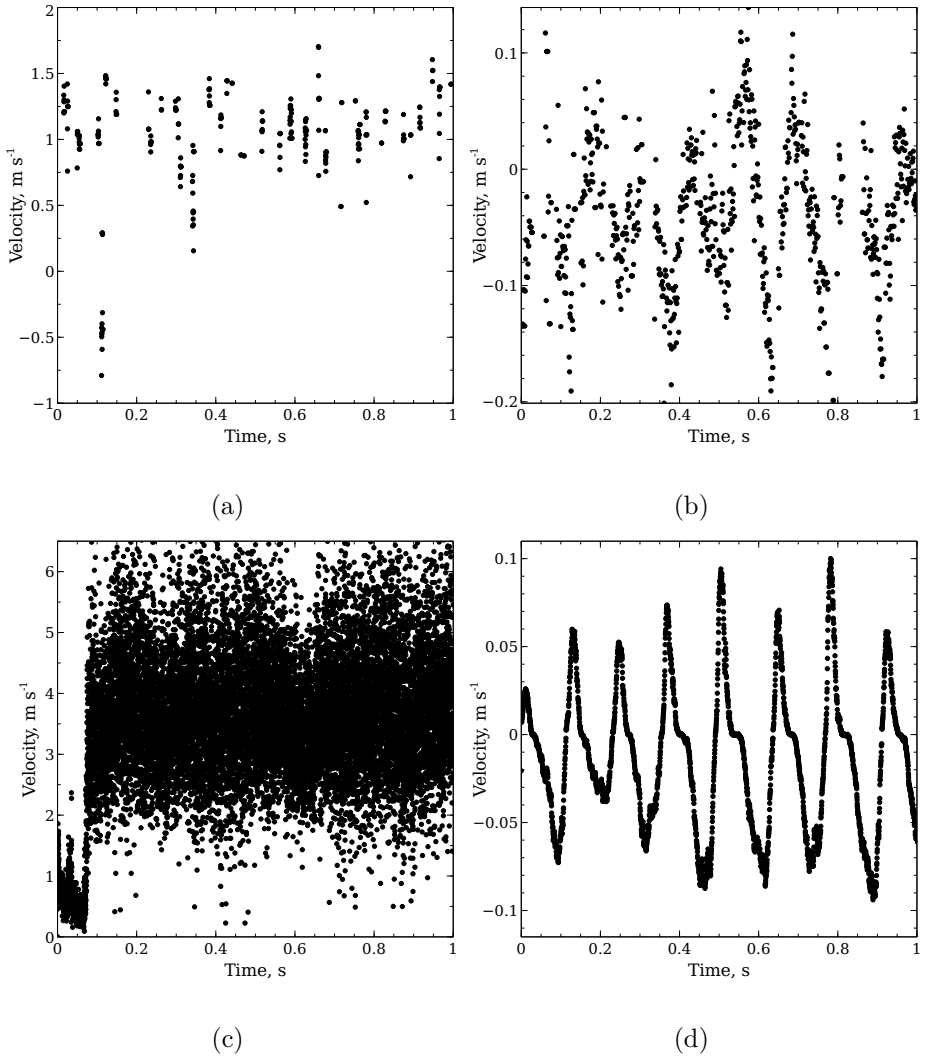


Figure 10: Velocity measurements for 4 mm glass beads (a) in the spout and (b) annular zone, and for irregular materials (c) in the spout and (d) annular zone.

than for the spherical particles due to the lower particle size of the irregular material. Furthermore, Figure 10(c) and Figure 10(d) also show that velocity values follow an oscillatory trend with a frequency of 7-8 Hz, which has also been observed by Mahmoodi et al.[17].

Once the dynamic evolution of the signal has been studied, the time averaged value allows obtaining the solid velocity profiles throughout the bed, which are the data to be compared in the steady state simulations and enables determining the amount of solid circulating thorough the system, i.e., the circulating solid flow rate. Figure 11(a) shows the axial solid velocity profile (at the contactor axis) for the glass beads. As observed, solids accelerate in the first stretch of the bed (close to the bottom), and they then decelerate until a peak velocity is reached. The deceleration is due to the solid cross-flow from the annulus into the spout, which leads to the sharing of the gas momentum with all the particles. Subsequent to the peak, there is a velocity descending trend for a bed stretch, and it then levels off until the value corresponding to the annulus bed surface (level $H_o$) is reached. Above this level (in the fountain), there is a sharp decrease in solid velocity as the spout expands to form the fountain.

In addition to the axial profile, radial velocity profiles can also be obtained. As an example, Figure 11(b) shows the velocities measured at a bed level of 20 cm for an operating velocity 10% above the minimum spouting velocity. As observed, velocity is maximum at the axis of the contactor, 1.25 $\mathrm{m\,s^{-1}}$, and it then goes on to descend as the measuring point is further from the axis of the bed. In the annular zone, there is a local minimum between the spout-annulus interface and the wall; that is, particles descend slower on the wall due to the wall-particle friction. These velocity profiles allow defining the position of the spout-annulus interface, as it is the place where the solid average velocity is zero, which in this case is close to 52% of the radius at the level of 20 cm.

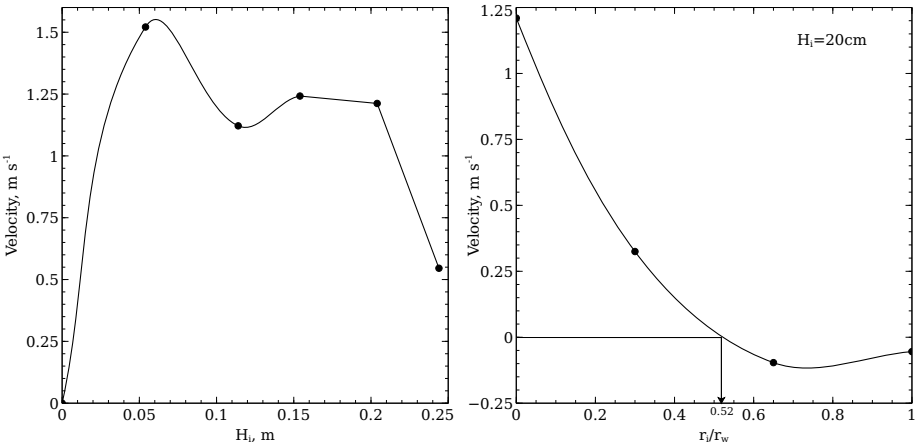


(a) (b)

Figure 11: Glass beads (a) axial velocity profile and (b) radial velocity profile at 20 cm from the bed bottom and $u/u_{ms} = 1.1$

These velocity profiles are the basis for determining other essential parameters in the operation with spouted beds, as are the average local velocity, the local solid flux, local solid momentum fluxes, average cycle times of the solids, and the overall particle circulation flow rate in the bed. In order to determine the local solid mass fluxes, porosity has to be ascertained through frame binarization or simulation. In the case of glass beads, assuming a porosity of 0.75 in the spout region, the axial profile in Figure 11(a) leads to a mass flux of 781 $\mathrm{kg\,m^{-2}\,s^{-1}}$. This information is crucial for the design of these beds for the treatment of a given solid flow rate.

## 4. Conclusions

A procedure based on borescopic particle image velocimetry has been designed, set up and tuned, and allows attaining reliable information of particle

velocity in conical spouted beds, with an estimated detection error below 10% for all cases and materials studied. Solid velocities in the 0-6.5 $\mathrm{m\,s^{-1}}$ range have been monitored in this study, which fall well below the recording capability of the camera. In fact, finer particles attain higher velocities, which would also be monitored by the technology proposed by simply increasing the recording speed. The methodology proposed allows also detecting velocity oscillations above the natural frequency of the system, which provide essential information on the transient behavior of the system. Thus, velocity oscillations are detected in the annular zone due to the incorporation of big particle clusters into the spout (cluster cross-flow from the annulus into the spout), along with the frequency at which this occurs. In addition, the annular zone oscillation frequency matches closely those reported in previous studies based on pressure fluctuations, which is an indication that velocity has been properly detected. Regarding the shape of the signal recorded, solid velocities in the spout follow a much more chaotic distribution, which depends on the amount of angular and/or linear momentum exchanged from the gas to the particle. Furthermore, this distribution also depends on both the collisions undergone by particles prior to and at the measurement point and the alignment of irregular particles along the spout.

A triggering criterion based on the beta distribution has been proposed for switching the algorithm for velocity monitoring according to bed density. Thus, based on the recordings, the algorithm corresponding to the measuring point is set, i.e., one for the dilute zone (usually in the spout) and a different one for the dense phase (annulus or clusters in the spout). In addition, the use of a spacer at the borescope tip is crucial for a good contrast between

particles and the background, specially in the dilute zones, in which there is a bubbly flow pattern and/or particles move upwards in the spout region. It is word mentioning that the number of particles detected in the dilute zone depends on the optics used and not on the implemented algorithm. The technology developed is highly flexible. Thus, when bigger particles than those used here must be monitored, the number of particles detected is increased by simply changing the lens between the borescope and the camera, and the subsequent velocity detection is straightforward without any change in the image treatment algorithm.

The tool developed based op the borescopic $PIV$ technique enables obtaining dynamic local data, which are highly relevant for comparing different systems or configurations or when local data are required for heat and mass transfer optimization or for model validation.

## Acknowledgments

This work has been carried out with the financial support from Spain's Ministry of Economy and Competitiveness (Projects $CTQ2016\text{-}75535\text{-}R$ and $RTI2018\text{-}098283\text{-}J\text{-}I00$), the European Regional Development Funds (ERDF) and the University of the Basque Country UPV/EHU ($US16/21$). Aitor Atxutegi is grateful for his Ph.D. grant from the University of the Basque Country UPV/EHU($PFI15\text{-}2017$).

## References

[1] H. Altzibar, G. Lopez, R. Aguado, S. Alvarez, M. J. San Jose, M. Olazar, Hydrodynamics of Conical Spouted Beds Using Different Types of Inter-

nal Devices, Chemical Engineering & Technology 32 (3) (2009) 463–469. doi:10.1002/ceat.200800605.
URL http://doi.wiley.com/10.1002/ceat.200800605

[2] P. K. Mollick, A. B. Pandit, P. K. Vijayan, Parameters Affecting Efficient Solid Circulation Rate in Draft Tube Spouted Bed, Industrial & Engineering Chemistry Research 57 (25) (2018) 8605–8611. doi:10.1021/acs.iecr.8b01691.
URL http://pubs.acs.org/doi/10.1021/acs.iecr.8b01691

[3] H. Nagashima, K. Suzukawa, T. Ishikura, Hydrodynamic performance of spouted beds with different types of draft tubes, Particuology 11 (5) (2013) 475–482. doi:10.1016/J.PARTIC.2013.01.007.
URL https://www.sciencedirect.com/science/article/pii/S167420011300103X?via%3

[4] H. Altzibar, I. Estiati, G. Lopez, J. F. Saldarriaga, R. Aguado, J. Bilbao, M. Olazar, Fountain confined conical spouted beds, Powder Technology 312 (2017) 334–346. doi:10.1016/J.POWTEC.2017.01.071.
URL https://www.sciencedirect.com/science/article/pii/S0032591017300918

[5] A. Pablos, R. Aguado, M. Tellabide, H. Altzibar, F. B. Freire, J. Bilbao, M. Olazar, A new fountain confinement device for fluidizing fine and ultrafine sands in conical spouted beds, Powder Technology 328 (2018) 38–46. doi:10.1016/J.POWTEC.2017.12.090.
URL https://www.sciencedirect.com/science/article/pii/S0032591017310483

[6] M. Olazar, M. San José, G. Zabala, J. Bilbao, New reactor in jet spouted

bed regime for catalytic polymerizations, Chemical Engineering Science 49 (24 PART A) (1994) 4579–4588. doi:10.1016/S0009-2509(05)80042-9.

[7] M. Olazar, J. Arandes, G. Zabala, A. Aguayo, J. Bilbao, Design and Operation of a Catalytic Polymerization Reactor in a Dilute Spouted Bed Regime, Industrial and Engineering Chemistry Research 36 (5) (1997) 1637–1643. doi:10.1021/ie960616q.

[8] G. Lopez, J. Alvarez, M. Amutio, A. Arregi, J. Bilbao, M. Olazar, Assessment of steam gasification kinetics of the char from lignocellulosic biomass in a conical spouted bed reactor, Energy 107 (2016) 493–501. doi:10.1016/J.ENERGY.2016.04.040.
URL https://www.sciencedirect.com/science/article/pii/S0360544216304467

[9] A. Erkiaga, G. Lopez, M. Amutio, J. Bilbao, M. Olazar, Steam gasification of biomass in a conical spouted bed reactor with olivine and $\gamma$-alumina as primary catalysts, Fuel Processing Technology 116 (2013) 292–299. doi:10.1016/J.FUPROC.2013.07.008.
URL https://www.sciencedirect.com/science/article/pii/S0378382013002397

[10] J. Alvarez, M. Amutio, G. Lopez, J. Bilbao, M. Olazar, Fast co-pyrolysis of sewage sludge and lignocellulosic biomass in a conical spouted bed reactor, Fuel 159 (2015) 810–818. doi:10.1016/J.FUEL.2015.07.039.
URL https://www.sciencedirect.com/science/article/pii/S0016236115007309?via%3

[11] G. Lopez, J. Alvarez, M. Amutio, N. Mkhize, B. Danon, P. van der Gryp, J. Görgens, J. Bilbao, M. Olazar, Waste truck-tyre processing by flash pyrolysis in a conical spouted bed reactor, Energy Conversion and Man-

agement 142 (2017) 523–532. doi:10.1016/J.ENCONMAN.2017.03.051.
URL https://www.sciencedirect.com/science/article/pii/S0196890417302637?via%3

[12] Z. Wang, C. J. Lim, J. R. Grace, H. Li, M. R. Parise, Effects of temperature and particle size on biomass torrefaction in a slot-rectangular spouted bed reactor, Bioresource Technology 244 (2017) 281–288. doi:10.1016/J.BIORTECH.2017.07.097.
URL https://www.sciencedirect.com/science/article/pii/S0960852417312130?via%3

[13] P. Mollick, R. Venugopalan, M. Roy, P. Rao, D. Sathiyamoorthy, P. Sengupta, G. Sharma, C. Basak, J. Chakravartty, Deposition of diversely textured buffer pyrolytic carbon layer in TRISO coated particle by controlled manipulation of spouted bed hydrodynamics, Chemical Engineering Science 128 (2015) 44–53. doi:10.1016/J.CES.2015.01.065.
URL https://www.sciencedirect.com/science/article/pii/S0009250915000949

[14] J. F. Saldarriaga, R. Aguado, A. Atxutegi, J. Bilbao, M. Olazar, Kinetic modelling of pine sawdust combustion in a conical spouted bed reactor, Fuel 227 (2018) 256–266. doi:10.1016/J.FUEL.2018.04.060.
URL https://www.sciencedirect.com/science/article/pii/S0016236118306926?via%3

[15] C. Moliner, F. Marchelli, B. Bosio, E. Arato, Modelling of Spouted and Spout-Fluid Beds: Key for Their Successful Scale Up, Energies 10 (11) (2017) 1729. doi:10.3390/en10111729.
URL http://www.mdpi.com/1996-1073/10/11/1729

[16] P. Kieckhefen, S. Pietsch, M. Höfert, M. Schönherr, S. Heinrich, F. Kleine Jäger, Influence of gas inflow modelling on CFD-DEM

simulations of three-dimensional prismatic spouted beds, Powder Technology 329 (2018) 167–180. doi:10.1016/j.powtec.2018.01.048.
URL http://linkinghub.elsevier.com/retrieve/pii/S0032591018300548

[17] B. Mahmoodi, S. H. Hosseini, M. Olazar, H. Altzibar, CFD-DEM simulation of a conical spouted bed with open-sided draft tube containing fine particles, Journal of the Taiwan Institute of Chemical Engineers 81 (2017) 275–287. doi:10.1016/j.jtice.2017.09.051.
URL http://linkinghub.elsevier.com/retrieve/pii/S1876107017305163

[18] Z. Rahimi-Ahar, M. S. Hatamipour, Hydrodynamics, numerical study and application of spouted bed, Reviews in Chemical Engineering 0 (0). doi:10.1515/revce-2017-0036.
URL http://www.degruyter.com/view/j/revce.ahead-of-print/revce-2017-0036/revc

[19] X. Bao, W. Du, J. Xu, An overview on the recent advances in computational fluid dynamics simulation of spouted beds, The Canadian Journal of Chemical Engineering 91 (11) (2013) n/a–n/a. doi:10.1002/cjce.21917.
URL http://doi.wiley.com/10.1002/cjce.21917

[20] S. Tebianian, K. Dubrawski, N. Ellis, R. A. Cocco, R. Hays, S. Reddy Karri, T. W. Leadbeater, D. J. Parker, J. Chaouki, R. Jafari, P. Garcia-Trinanes, J. P. Seville, J. R. Grace, Investigation of particle velocity in FCC gas-fluidized beds based on different measurement techniques, Chemical Engineering Science 127 (2015) 310–322. doi:10.1016/J.CES.2015.01.049.
URL https://www.sciencedirect.com/science/article/pii/S0009250915000780

[21] M. Olazar, M. J. SanJose, R. Aguado, J. Bilbao, Solid flow in jet spouted beds, Industrial & Engineering Chemistry Research 35 (8) (1996) 2716–2724, wOS:A1996VB61000026. doi:10.1021/ie950500e.

[22] X. Yang, J. R. van Ommen, E. Wagner, R. F. Mudde, Time-resolved characterization of a flat-base spouted bed with a high speed X-ray system, Chemical Engineering Journal 254 (2014) 143–152. doi:10.1016/J.CEJ.2014.05.050.
URL https://www.sciencedirect.com/science/article/pii/S1385894714006251

[23] H. C. Park, H. S. Choi, Visualization of flow structures inside a conical spouted bed by electrical capacitance volume tomography, Particuologydoi:10.1016/j.partic.2018.01.002.
URL http://linkinghub.elsevier.com/retrieve/pii/S1674200118300683

[24] M. Bieberle, F. Barthel, Combined phase distribution and particle velocity measurement in spout fluidized beds by ultrafast X-ray computed tomography, Chemical Engineering Journal 285 (2016) 218–227. doi:10.1016/J.CEJ.2015.10.003.
URL https://www.sciencedirect.com/science/article/pii/S1385894715013789?via%3

[25] T. Al-Juwaya, N. Ali, M. Al-Dahhan, Investigation of cross-sectional gas-solid distributions in spouted beds using advanced non-invasive gamma-ray computed tomography (CT), Experimental Thermal and Fluid Science 86 (2017) 37–53. doi:10.1016/j.expthermflusci.2017.03.029.
URL http://linkinghub.elsevier.com/retrieve/pii/S0894177717300912

[26] N. Ali, T. Al-Juwaya, M. Al-Dahhan, An advanced evaluation of spouted beds scale-up for coating TRISO nuclear fuel particles using Radioactive Particle Tracking (RPT), Experimental Thermal and Fluid Science 80 (2017) 90–104. doi:10.1016/J.EXPTHERMFLUSCI.2016.08.002.
URL https://www.sciencedirect.com/science/article/pii/S0894177716302072

[27] L. Spreutels, B. Haut, R. Legros, F. Bertrand, J. Chaouki, Experimental investigation of solid particles flow in a conical spouted bed using radioactive particle tracking, AIChE Journal 62 (1) (2016) 26–37. doi:10.1002/aic.15014.
URL http://doi.wiley.com/10.1002/aic.15014

[28] G. Mohs, O. Gryczka, S. Heinrich, L. Mörl, Magnetic monitoring of a single particle in a prismatic spouted bed, Chemical Engineering Science 64 (23) (2009) 4811–4825. doi:10.1016/J.CES.2009.08.025.
URL https://www.sciencedirect.com/science/article/pii/S0009250909005740?via%3

[29] E. E. Patterson, J. Halow, S. Daw, Innovative Method Using Magnetic Particle Tracking to Measure Solids Circulation in a Spouted Fluidized Bed, Industrial & Engineering Chemistry Research 49 (11) (2010) 5037–5043. doi:10.1021/ie9008698.
URL http://pubs.acs.org/doi/abs/10.1021/ie9008698

[30] D. A. Santos, G. C. Alves, C. R. Duarte, M. A. S. Barrozo, Disturbances in the Hydrodynamic Behavior of a Spouted Bed Caused by an Optical Fiber Probe: Experimental and CFD Study, Industrial & Engineering Chemistry Research 51 (9) (2012) 3801–3810. doi:10.1021/ie2023838.
URL http://pubs.acs.org/doi/10.1021/ie2023838

[31] M. Olazar, M. J. San José, S. Alvarez, A. Morales, J. Bilbao, Measurement of Particle Velocities in Conical Spouted Beds Using an Optical Fiber Probedoi:10.1021/IE9800243.
URL https://pubs.acs.org/doi/abs/10.1021/ie9800243

[32] L. Qian, Y. Lu, W. Zhong, B. Jin, Developing a High Speed Fiber-optic Endoscopic Technique for Measuring Particle Phase Characteristics in a Spouted Bed, Procedia Engineering 102 (2015) 150–158. doi:10.1016/J.PROENG.2015.01.118.
URL https://www.sciencedirect.com/science/article/pii/S1877705815001198

[33] J. Yang, R. W. Breault, J. M. Weber, S. L. Rowan, Determination of flow patterns by a novel image analysis technique in a rectangular spouted bed, Powder Technology 334 (2018) 151–162. doi:10.1016/j.powtec.2018.04.067.
URL http://linkinghub.elsevier.com/retrieve/pii/S0032591018303486

[34] F. Shaffer, B. Gopalan, R. W. Breault, R. Cocco, S. R. Karri, R. Hays, T. Knowlton, High speed imaging of particle flow fields in CFB risers, Powder Technology 242 (2013) 86–99. doi:10.1016/J.POWTEC.2013.01.012.
URL https://www.sciencedirect.com/science/article/pii/S0032591013000296?via%3

[35] H. Gao, X. Gong, G. Hu, Statistical and frequency analysis of pressure fluctuation in an annular spouted bed of coarse particles, Powder Technology 317 (2017) 216–223. doi:10.1016/j.powtec.2017.05.007.
URL http://linkinghub.elsevier.com/retrieve/pii/S0032591017303819

[36] S. Tebianian, K. Dubrawski, N. Ellis, R. A. Cocco, R. Hays, S. R. Karri, T. W. Leadbeater, D. J. Parker, J. Chaouki, R. Jafari, P. Garcia-Trinanes, J. P. Seville, J. R. Grace, Solids flux measurements via alternate techniques in a gas-fluidized bed, Chemical Engineering Journal 306 (2016) 306–321. doi:10.1016/J.CEJ.2016.07.058.
URL https://www.sciencedirect.com/science/article/pii/S138589471631004X

[37] B. Gopalan, F. Shaffer, A new method for decomposition of high speed particle image velocimetry data, Powder Technology 220 (2012) 164–171. doi:10.1016/J.POWTEC.2011.09.001.
URL https://www.sciencedirect.com/science/article/pii/S0032591011004694?via%3

[38] H. Hessenkemper, T. Ziegenhein, Particle Shadow Velocimetry (PSV) in bubbly flows, International Journal of Multiphase Flow- doi:10.1016/j.ijmultiphaseflow.2018.04.015.
URL http://linkinghub.elsevier.com/retrieve/pii/S0301932217308662

[39] H. Altzibar, G. Lopez, J. Bilbao, M. Olazar, Minimum Spouting Velocity of Conical Spouted Beds Equipped with Draft Tubes of Different Configuration, Industrial & Engineering Chemistry Research 52 (8) (2013) 2995–3006. doi:10.1021/ie302407f.
URL http://pubs.acs.org/doi/10.1021/ie302407f

[40] H. Altzibar, G. Lopez, I. Estiati, J. Bilbao, M. Olazar, Particle Cycle Times and Solid Circulation Rates in Conical Spouted Beds with Draft Tubes of Different Configuration, Industrial & Engineering Chemistry Research 52 (45) (2013) 15959–15967. doi:10.1021/ie401412j.
URL http://pubs.acs.org/doi/10.1021/ie401412j

[41] L. Zhang, Z. Wang, S. Li, H. Qin, Effect of a draft tube on oil shale particle drying process of a spouted bed: CPFD simulation studies, Advanced Powder Technology 29 (9) (2018) 2255–2267. doi:10.1016/J.APT.2018.06.010.
URL https://www.sciencedirect.com/science/article/pii/S0921883118302747?via%3

[42] M. Cortazar, G. Lopez, J. Alvarez, M. Amutio, J. Bilbao, M. Olazar, Advantages of confining the fountain in a conical spouted bed reactor for biomass steam gasification, Energy 153 (2018) 455–463. doi:10.1016/J.ENERGY.2018.04.067.
URL https://www.sciencedirect.com/science/article/pii/S0360544218306741?via%3

[43] G. Farnebäck, Two-Frame Motion Estimation Based on Polynomial Expansion, SCIA'03 Proceedings of the 13th Scandinavian conference on Image analysis 2003 (1) (2003) 363–370.